

## MODELING THE EFFECT OF SPRAY/WALL IMPINGEMENT ON COMBUSTION PROCESS AND EMISSION OF DI DIESEL ENGINE

by

**Samad JAFARMADAR, Shram KHALILARYA,  
Sina SHAFEE, and Ramin BARZEGAR**

Original scientific paper  
UDC: 621.43.041.6:66.011  
DOI: 10.2298/TSCI0903023J

*This work is presented to study the effect of spray impinging on the combustion process and emissions in a direct injection diesel engine at various engine speeds. Computations are carried out using a three-dimensional modeling for sprays, spray-wall interactions, flow field, emission, and combustion process. Results indicate an increase in engine speed leads to increased spray impinging (wall film formation), turbulence intensity and average wall temperature in cylinder. The enhanced air/fuel mixing and intensified evaporation of wall film decreases soot emission by reducing the extent of the fuel rich regions specially in impinging zones. Also at higher engine speeds, combustion is delayed and fuel is consumed in a shorter time period by the enhanced air and fuel mixing. The shorter combustion duration provides less available time for soot and NO<sub>x</sub> formations. However, only a few attempts have been made to address the effect of impingement of spray with piston walls on the emissions and combustion process. The results of model in addition to approving the corresponding data in the literature are also compared with the experimental data and shown good agreement.*

Key words: diesel engine, impinging, wall film, combustion, spray, emission

### Introduction

In a very competitive world improvement of engine performance has become an important issue for automotive manufacturers. In order to improve the engine performance, the combustion process is now being studied in more detail. Also, the recent global environmental regulations for reducing engine emissions have forced engine designers to explore new engine concepts and to study the effect of engine parameters on the formation of pollutant emissions. Simulation of the combustion system by means of computer modeling makes it possible to explore combustion regimes that may be difficult and/or expensive to achieve with experiments [1].

Such modeling first started out in 1950 with simple thermodynamical models for engine cycles which then were extended in 1970 to multi-zone models. Nowadays with the progressive development of computational fluid dynamics (CFD) and flow field models, it is also possible to study and predict droplet distribution, temperature, pressure, and other parameters at every desired point and time within the combustion chamber.

Flow field models, such as KIVA II code in 1990 [2, 3] and numerical Ricardo code in 1992 which was employed to investigate an optimum value for gas fuel injector angle in a dual fuel diesel-gas engine to obtain minimum unburned hydrocarbon (UHC) emissions [4], are premiere examples. Choi *et al.* [5] used STARCD code and particle image velocimetry (PIV) analy-

sis to study in-cylinder flow field of a single cylinder DI diesel engine. It was indicated that high Reynolds  $k-\varepsilon$  turbulent model pretty much satisfies such flow fields.

Uludogan *et al.* studied the operation of a small DI diesel engine over a large range of engine speeds (2000-12000 rpm) by using a multidimensional computer code to study the effect of speed and injection timing engine power, emission trade-off and so on but spray wall impingement has not been fully taken in account. It was shown such high speed is predicted to decrease soot and  $\text{NO}_x$  formation and increase combustion efficiency and engine cycle power [1].

3D KIVA code has also been used by Patterson *et al.* to study the effects of injection pressure and split injections on diesel engine performance and soot and  $\text{NO}_x$  emissions. The results show the use of the updated version of KIVA gives good agreement between measured and predicted engine cylinder pressures and heat release data for single injection cases [6]. By use of a modified version of the CFD code FLUENT, Meingast *et al.* have analyzed spray/wall interaction on a flat wall under diesel engine like conditions. The penetration behavior of the spray as well as droplet velocity and diameter and the wall heat flux were measured varying injection pressure, distance between nozzle and wall, gas density, and wall temperature. It was shown that the fluid dynamics changes due to higher droplet velocity prior to impingement and improved wall models need to be derived from experiments conducted under well known boundary conditions similar to diesel engine conditions [7]. The research group of Reitz of University of Wisconsin, Madison, performed modeling the combustion in a quiescent chamber engine, in order to evaluate the  $\text{NO}_x$  particulate trade-off, varying the injection timing, the injection pressure and the split injection dwell angle. Comparing with measured data, computations show that soot and  $\text{NO}_x$  emissions increase at low injection pressures. Results also indicate that, when compared to the single injection case, an additional high temperature region is observed between the separate spray clouds with split injection [8].

A series of experiments were performed by Yoshizaki *et al.* in a high-pressure constant volume bomb using a diesel spray impinging onto the simulated piston. The spray outlines were recorded as a function of time from various directions. Three-dimensional distributions of the impinged sprays were obtained by analyzing the photographs taken from these various directions. The measured spray outlines were compared with the calculated results of the spray model based on the multi-package model. The calculated spray outlines were in reasonably good agreement with the measured outline [9]. In some DI engines, the fuel spray has been intentionally impinged on a surface as a method to control combustion. One early system which used such a technique was the M-combustion developed by MAN [10], in which the fuel is injected on the surface of the piston bowl, forming a liquid film. Vaporization of this film controls the rate of combustion allowing the use of low cetane number fuels. Detailed investigations of wall-spray development are reported in Mohammadi *et al.* [11] and Allocca *et al.* [12].

At the present work a three dimensional CFD code has been used to predict and study the effects of impinging spray on the combustion process and emissions at different engine speeds in the OM-355 diesel engine. This paper also demonstrates the usefulness of multidimensional models to gain insight into the combustion process and to provide direction for exploring new engine concepts. The results of this model are approved by the corresponding data in the literature [1, 13].

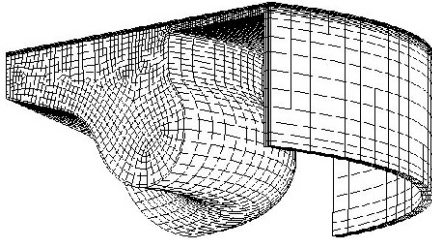
## Model formulation

The numerical model for heavy duty OM-355 diesel engine with the specifications on tab. 1 is carried out using AVL Fire code. It is old diesel engine and its fuel injection system is low pressure. Start of injection pressure is 195 bar and the injection period starts from  $-18^\circ\text{CA}$

**Table 1. Engine specifications (OM-355 Mercedes Benz)**

Engine type	Heavy duty DI diesel engine
Number of injector holes	4
Engine speed at max torque	1400 rpm
Engine speed at max power	2200 rpm
Piston diameter stroke	128 150 mm
Cylinder volume	11.58 litre
Heavy duty DI diesel engine	Nozzle opening pressure: 195 bar
Maximum output power	176.5 kW (240 hp)
Maximum outlet torque	824 Nm
Number of cylinders	6, vertical type
Compression ratio	16.1:1
Angle of fuel injection	150°
Injection system: low-pressure, linear pump	Maximum injection pressure: 500 bar

up to 0 °C. Calculations are carried out on the closed system from intake valve closure at –118 °CA to exhaust valve open (EVO) at 120 °CA. There is a centric injector with four holes, mounted beneath cylinder head and fuel is injected at a constant rate. Initial pressure value is chosen as intake pressure and initial temperature is calculated by ideal gas law meanwhile air-fuel ratio modeling equals to experimental. Swirl ratio is assumed to be quiescent condition and considering the symmetry of the model, problem is only solved for one fourth section of the

**Figure 1. View of the computational mesh**

whole geometry. Figure 1 shows the numerical grid. The Fire software solves the compressible, turbulent, three dimensional transient conservation equations for reacting multi-component gas mixtures with the flow dynamics of an evaporating liquid spray. The turbulent flows within the combustion chamber are simulated using the RNG  $k-\varepsilon$  turbulence model, modified for variable-density engine flows.

Combustion process is modeled by Eddy Breakup model. This model assumes that in pre-mixed turbulent flames, the reactants (fuel and oxygen) are contained in the same eddies and are separated from eddies containing hot combustion products. The rate of dissipation of these eddies determines the rate of combustion:

$$\overline{\rho \dot{r}_{fu}} = \frac{C_{fu}}{\tau_R} \bar{\rho} \min. \bar{y}_{fu}, \frac{\bar{y}_{ox}}{S} \cdot \frac{C_{pr} \bar{y}_{pr}}{1 S} \quad (1)$$

The first two terms of the “minimum value of” operator determine whether fuel or oxygen is present in limiting quantity, and the third term is a reaction probability which ensures that the flame is not spread in the absence of hot products [14]. Above equation includes three constant coefficients ( $C_{fu}$ ,  $\tau_R$ ,  $C_{pr}$ ) and  $C_{fu}$  varies from 3 to 25 in diesel engines. An optimum value was selected according to experimental data [15].

Spray breakup and droplet distribution is modeled by advanced wave standard [14]. In this model the growth of an initial perturbation on a liquid surface is linked to its wave length and to other physical and dynamic parameters of the injected fuel and the domain fluid.

Drop parcels are injected with characteristic size equal to the nozzle exit diameter (blob injection). The Dukowicz model was applied for treating the heat-up and evaporation of the droplets, which is described in [16]. This model assumes a uniform droplet temperature. In addition, the rate of droplet temperature change is determined by the heat balance, which states that the heat convection from the gas to the droplet either heats up the droplet or supplies heat for vaporization.

$\text{NO}_x$  formation is modeled by the Zeldovich mechanism while soot formation is modeled by Kennedy, Hiroyasu and Magnussen mechanism [13].

### Wall film model

Due to imperfect atomization and evaporation, a portion of the injected spray droplets impact on the walls of the combustion chamber and in special conditions, lead to formation of a wall film. This influences the combustion process and consequently the production of emissions, as an incomplete combustion in the vicinity of the wall will result in high hydrocarbon and soot emissions. The spray-wall interaction model used in the simulations was based on the spray-wall impingement model described in [13, 14, 17]. At this model, behavior of the impinging droplet is influenced by major factors like wall temperature and Weber number which identifies a number of impingement regimes. In principle, higher surface temperatures prevent the formation of wall film due to rapid boiling or due to droplet re-bouncing because of the Leiden frost phenomenon [13, 14]. To gain insight into this fact, a code was written and integrated with the AVL Fire Solver to calculate the mean cylinder surface temperature at desired crank angle.

There are four spray-wall interaction regimes depending on the inlet droplet velocity. At very low inlet velocities the droplet sticks to the wall or to the wall film.

When the inlet velocity increases a vapor or gas boundary layer is trapped underneath the droplet and causes the liquid to rebound. During the rebound, parts of the kinetic energy are dissipated and the outgoing normal velocity is usually lower than the incoming normal velocity. A further increase of the velocity leads either to the spread or the splash regime. In the spread regime the complete liquid spreads along the wall with hardly any normal velocity. In the splash regime a part of the liquid remains near the surface and the rest of it is reflected and broken up into secondary droplets. Figure 2 presents the reflection of a parcel containing droplets at the wall. The wall film module takes care of the splashing regime of impinging droplets.

According to correlations by Mundo *et al.* [18, 19], the predominant influence of droplet momentum and properties as viscosity and surface tension is taken into consideration by introducing the dimensionless groups Reynolds number and Ohnesorge number for the particular droplet:

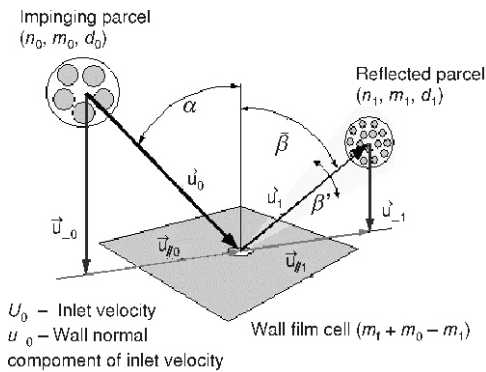


Figure 2. Wall interaction of droplets

$$\text{Re}_D = \frac{\rho d_0 u_0}{\mu} \quad (2)$$

$$\text{Oh} = \frac{\mu}{\sqrt{\rho \sigma d_0}} \quad (3)$$

The Reynolds number compares momentum to viscous forces, whereas the Ohnesorge number relates viscous forces to surface tension. For the Reynolds number, only the wall normal component  $u_0$  of the initial droplet velocity  $u_0$  is used, which accounts for impact angle effects. In addition to the Weber number, a  $K$ -value [18] is defined which is a modified form of a Weber number:

$$\text{We} = (\text{Re}_D \cdot \text{Oh})^2 \quad (4)$$

$$K = \text{Oh} \cdot \text{Re}_D^{0.125} \quad (5)$$

This  $K$ -value is a characteristic quantity which serves to distinguish between different impingement regimes and generally is used as the key parameter for the splashing model. The criterion for inception of splashing is given at  $K = 57.7$ . Consequently, for  $K < 57.7$ , the droplets are deposited completely at the wall without bouncing or breakup and the kinetic energy of the droplet is dissipated. In the splashing regime ( $K > 57.7$ ) with increasing droplet impact-momentum, a larger mass fraction is atomized and reflected. During this splashing the droplets are partially shattered to produce a different droplet size spectrum for the reflected droplets. With increasing  $K$  (higher momentum, less surface tension), the reflected droplets tend to be smaller and have a narrower bandwidth of size distribution.

## Results and discussion

Results are presented in figures and contours at a horizontal section just above the piston bowl. For the contours, engine speeds of 1400 rpm and 1600 rpm as low, and 2000 rpm and 2200 rpm are chosen as higher speed ranges.

Figures 3, 4, 5, and 6, respectively, show computed pressure, temperature, heat release rate (HRR), and turbulence intensity in cylinder. The presented figures show global (cylinder averaged) quantities as a function of time (crank angle) during the closed cycle. As can be seen at these figures when engine speed increase, due less time available, short combustion duration and improved air-fuel mixing and induced higher turbulence intensity, combustion start with de-

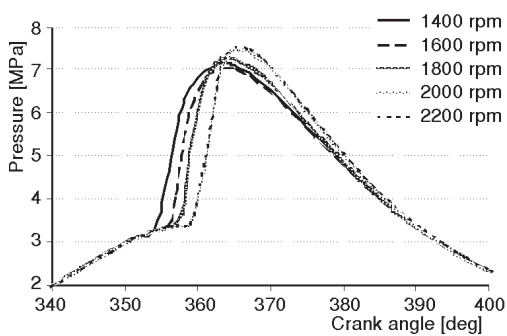


Figure 3. Mean in-cylinder pressure vs. crank angles at different engine speeds

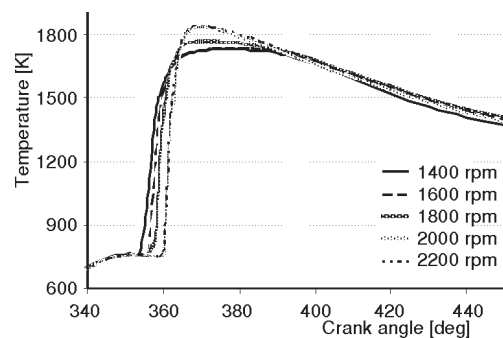


Figure 4. Mean in-cylinder temperature vs. crank angles at different engine speeds

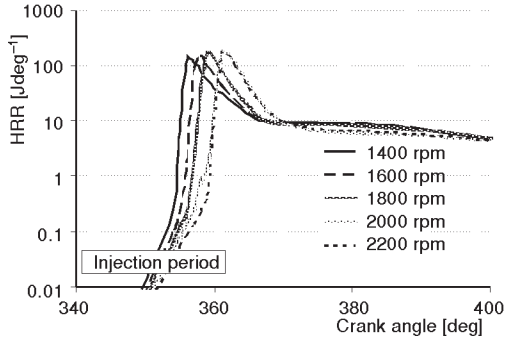


Figure 5. Heat release rate for varying engine speed at different crank angles

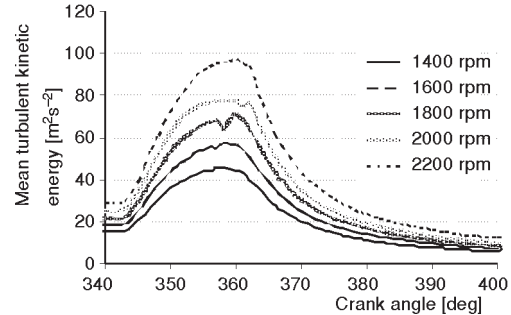


Figure 6. Mean turbulence intensity vs. crank angle at different engine speeds

lay near top dead centre (TDC). Therefore the peak values for pressure, temperature, and premix burning are increased. Combustion process has started near TDC for 1400 rpm and 1600 rpm but due long ignition delay, it is postponed to approximately  $5^\circ$  aTDC at 2000 rpm and 2200 rpm.

Figure 6 shows turbulence intensity vs. crank angle at various engine speeds. It can be realized from this figure that at higher engine speed turbulence intensity increases approaching TDC, which is a result of combustion process occurring and would increase air-fuel mixing subsequently.

Figures 7, 13, and 14 show computed and measured in cylinder pressures and exhaust emission for OM355 DI diesel engine [15]. The operating condition is 1400 rpm and full load state. As can be seen, there is a good agreement between the measured data and the model prediction. The good agreement between the measured and computed results for this engine operating condition (maximum emission revolution) gives confidence in the model predictions, and suggests that the model may be used to explore new engine concepts.

Figures 8, 9, 10, and 17 show mass impinging, average temperature on piston surface, wall film evaporated, and velocity vector in cylinder at various engine speeds, respectively. The

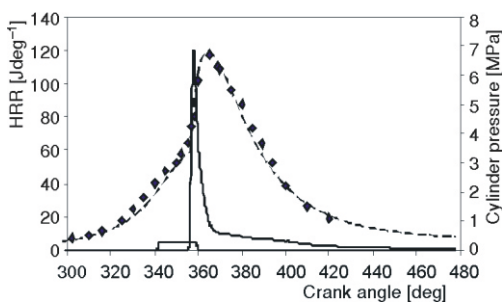


Figure 7. Heat release rate, injection mode and comparison of calculated and measured [15] in cylinder pressure at 1400 rpm

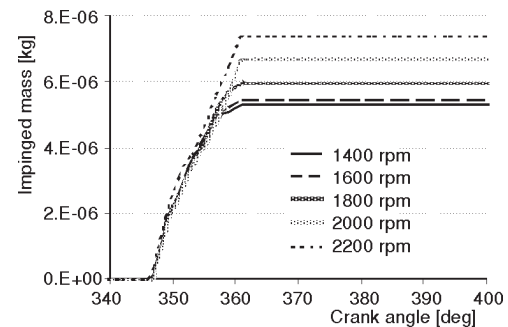


Figure 8. Impinged mass at different engine speeds vs. crank angle

increase in engine speed shortens the available time for the spray evaporating and leads to more impinged mass and high wall temperature (as shown in figs. 8 and 15). Also at high engine speed, because of high temperature in cylinder and low heat loss, piston surface temperature will increase (as shown in fig. 9). Impingement of spray has started approximately  $4^\circ$ CA after injec-

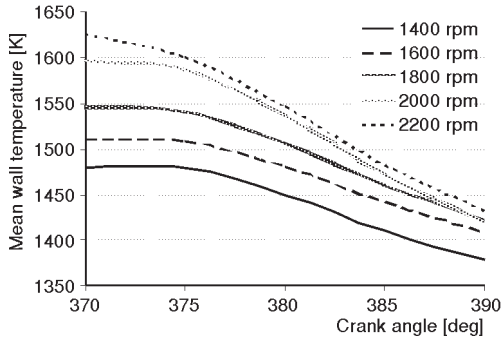


Figure 9. Mean wall temperature vs. crank angle for different engine speeds

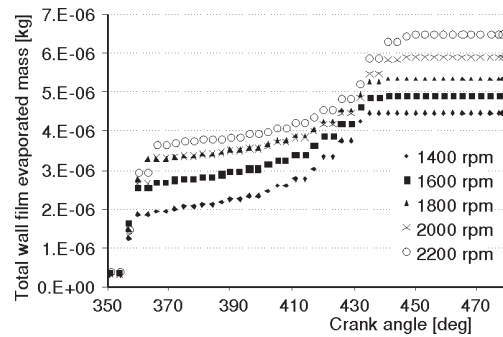


Figure 10. Total wall film mass evaporated vs. crank angle at different engine speeds

tion and is continued over the injection period. Furthermore, contact with a hot wall at high engine speeds intensifies wall film evaporation (as shown in figs. 10 and 16). The formation of a large-scale gas vortex near the wall at enhanced turbulence intensity region may also promote air entrainment and enhance mixture formation (shown in figs. 6 and 17). Therefore in the impinging zones, soot mass fraction decreases even more.

Figures 11 and 12 show the computed  $NO_x$  and soot mass fraction. There is a substantial reduction in soot mass fraction at higher engine speeds while  $NO_x$  mass fraction does not reduce considerably. Under high temperature and fuel rich region, as typically found in diesel engine combustion, hydrocarbon fuels exhibit a strong tendency to form carbonaceous particles or soot. Peak value for soot occurs approximately at 380 °CA but usually, under engine running

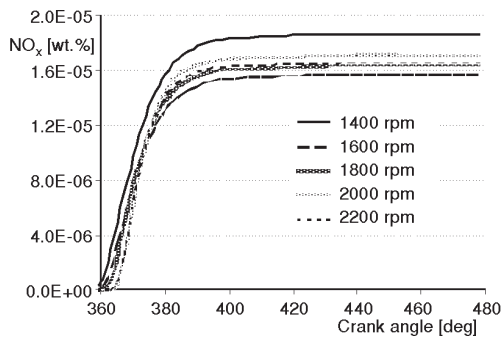


Figure 11.  $NO_x$  mass fraction vs. crank angles at different engine speeds

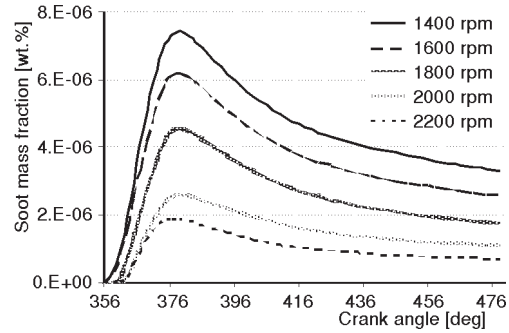


Figure 12. Soot mass fraction vs. crank angles at different engine speeds

conditions, most of the soot formed in the early stages of the combustion process is depleted due to oxidation. The area which the equivalence ratio is close to 1 and the temperature is higher than 2000 K is the  $NO_x$  formation area. In addition, the area at which the equivalence ratio is higher than 3 and the temperature is approximately between 1600 K and 2000 K is the soot formation region.

At higher engine speeds due to less time availability and higher in cylinder temperature (above 2000 K),  $NO_x$  mass fraction decreases to some extent [1]. Similarly, the reduction of the soot is also because of the reduced available time and the leaner air/fuel mixture because of enhanced turbulence intensity along with enhanced wall film evaporation near wall. It seems

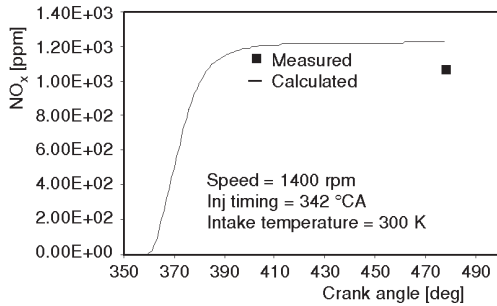


Figure 13. Comparison of calculated and measured [15]  $\text{NO}_x$  emission

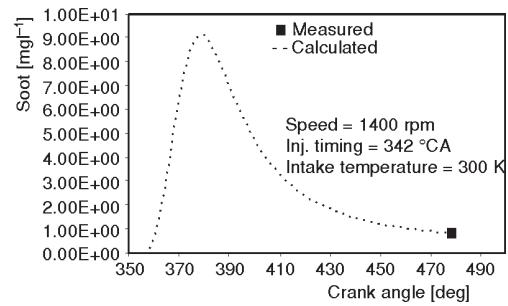


Figure 14. Comparison of calculated and measured [15] soot emission

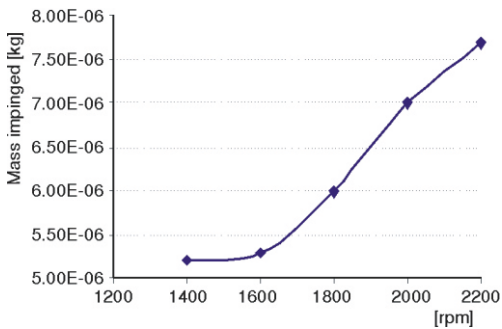


Figure 15. Final impinged mass values at different engine speeds

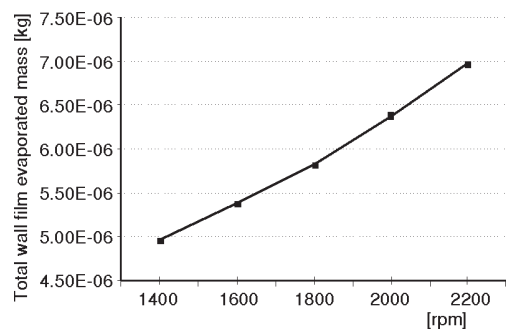


Figure 16. Final evaporated wall film mass value at different engine speeds

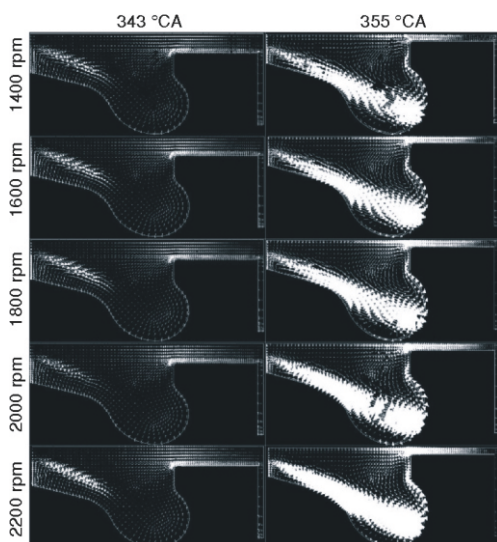


Figure 17. Velocity vectors at two crank angles for all speed cases

from these figures that the higher engine speed is a possible solution to simultaneously reduce soot and  $\text{NO}_x$  emissions in direct injection diesel engines [1].

Figures 18 shows spray distribution, wall-impingement, and fuel vapor contours over injection period crank angles. Two different cross-sections are used at horizontal and vertical planes perpendicular to cylinder axis inside the bowl and diagonally across bowl accordingly. As mentioned above, the increase of engine speed shortens the available time for the spray to evaporate thus, it is seen that fuel vapor decreases at each crank angle.

Also as indicated in this figure, the near wall region includes lean mixture because of turbulent mixing and enhanced wall film evaporating.

Figures 19 and 20 show the contours of  $\text{NO}_x$  and soot, respectively, at several crank angles

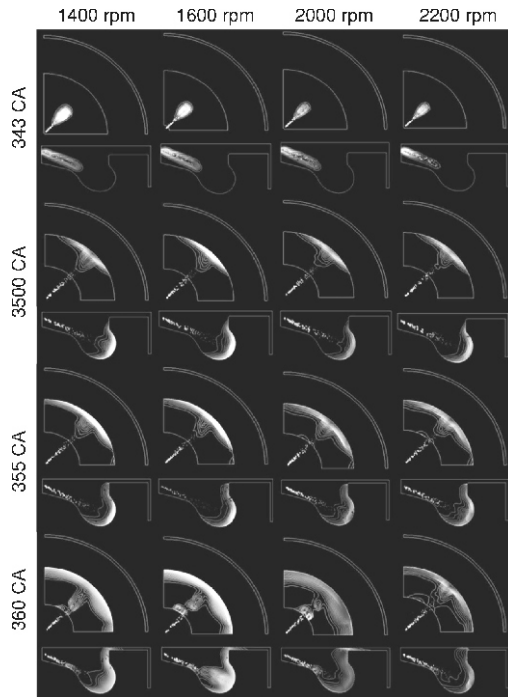


Figure 18. Plots of fuel spray, vapor, and wall-impingement at different crank angles over engine speeds

in one cross-section taken diagonally across the bowl and splitting it in half. On the whole, the opposing behavior of  $\text{NO}_x$  and soot formation is explicit from both contours, which means that in regions with higher  $\text{NO}_x$  concentrations, soot tends to be less and *vice versa*.

Observing both previous temperature contours (fig. 21) and this figure simultaneously,  $\text{NO}_x$  concentration seems to increase at locals with high temperature (above 2000 K) which agrees well with data in literature. Mean  $\text{NO}_x$  concentration is retained at peak value but extended to whole combustion chamber in 478 °CA (EVO).

Figure 20 indicates soot concentration at different engine speeds for several crank angles. Soot formation also starts over TDC and increases with crank angle. The maximum local concentration of soot are observed in regions where fuel vapor contours indicate rich mixtures (equivalence ratio is higher than 3)

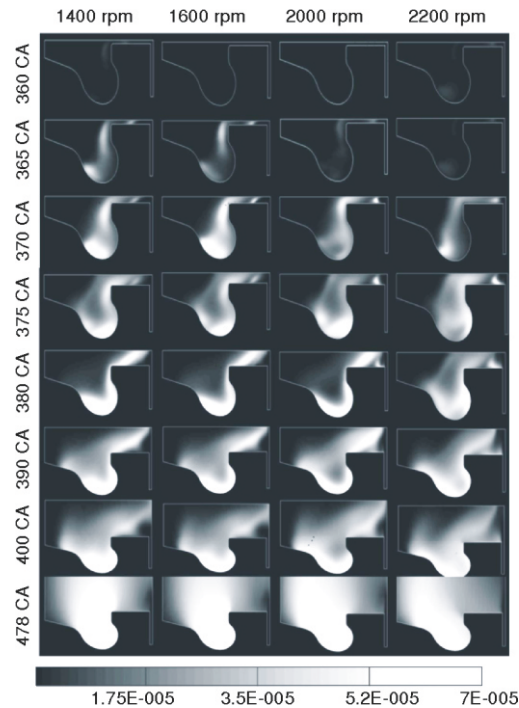


Figure 19. Contours of  $\text{NO}_x$  concentration at different crank angles over engine speeds

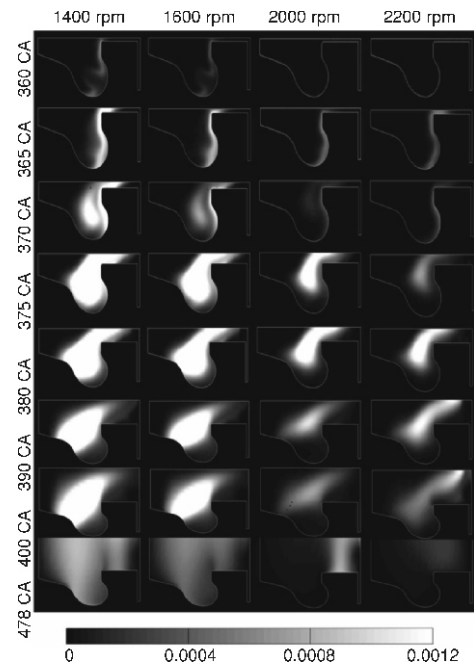
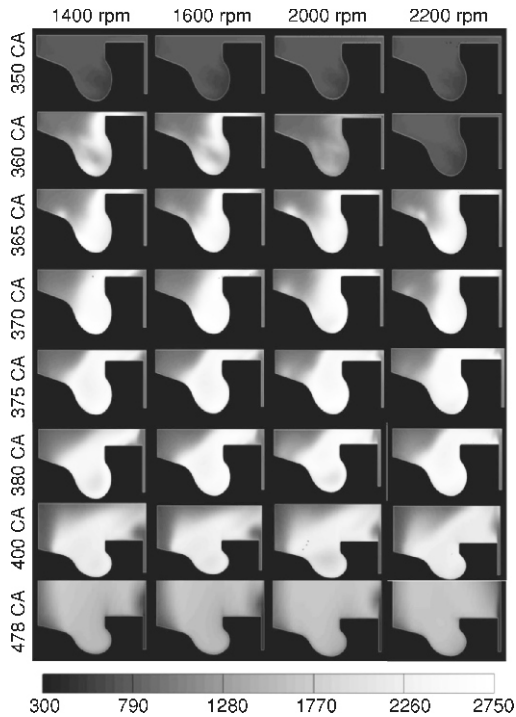


Figure 20. Contours of soot concentration at different crank angles over engine speeds



**Figure 21. Temperature contours for selected engine speeds over various crank angles**

Spray impinging at high engine speeds is increasing due to more fuel injection and less time available for droplet evaporation of the spray.

At higher engine speeds, turbulence intensity and average piston surface temperature increases. Therefore wall film evaporation is intensified and mixture formation is optimized.

Because of less available time, high wall temperature, more spray impinging, high turbulence intensity and fast mixture formation on impinging zones at high engine speeds, soot concentrations tend to decrease substantially without a considerable change in  $\text{NO}_x$  formation.

## Nomenclature

$C$	– empirical coefficient, [kg]
$\dot{V}$	– fuel consumption rate, [ $\text{kg s}^{-1}$ ]
$S$	– stoichiometric oxygen requirement, [–]
$\bar{y}$	– mass fraction

### Greek letters

$\mu$	– viscosity, [ $\text{kg m}^{-1} \text{s}^{-1}$ ]
$\rho$	– density, [ $\text{kg m}^{-3}$ ]

$\sigma$	– surface tension, [ $\text{Nm}^{-1}$ ]
$\tau_R$	– turbulent mixing time scale, [s]

### Subscripts

fu	– fuel
ox	– oxidizer
pr	– product
R	– reaction

bowl edge which are farther from injector will be where high concentration of soot are seen. It is found out that soot mass fraction in each crank angle, reduces with increasing speed due to the shorter time period of combustion which provides much less available time for particle formation. Also at the impinging zone soot mass fraction decreased.

## Summery and conclusions

At this paper was dedicated to study the effect of spray impinging on combustion process and emissions in a DI diesel engine at various engine speeds using AVL Fire 8.3 software and the following results are obtained.

Results of model for in cylinder pressure and exhaust emission at 1400 rpm and full load state (maximum emission point) is compared with the corresponding experimental data and show good agreement. Such verification between the measured and computed result for this operating point gives confidence in the model prediction, and suggest that the model may be used to explore new engine concepts.

## References

- [1] Uludogan, A., Foster, D. E., Reitz, R. D., Modeling the Effect of Engine Speed on the Combustion Process and Emissions in a DI Diesel Engine, SAE paper 962056

- [2] Heywood, J. B., Internal Combustion Engine Fundamental, McGraw Hill Book Company, New York, USA, 1988
- [3] Gosman, A. D., Computer Modeling of Flow and Heat Transfer in Engines, Progress and Prospects, Imperial College of Science and Technology, London
- [4] Jeske Felix, R., *et al.*, Modeling of the Natural Gas Injection Process in a Two-Stroke Diesel Engine, SAE Paper 920192
- [5] Choi, W., *et al.*, In-Cylinder Flow Field Analysis of a Single Cylinder DI Diesel Engine Using PIV and CFD, SAE paper 2003-01-1846
- [6] Patterson, M. A., *et al.*, Modeling the Effects of Fuel Injection Characteristics on Diesel Engine Soot and NOx Emissions, SAE paper 940523
- [7] Meingast, U., Staudt, M., *et al.*, Analysis of Spray/Wall Interaction under Diesel Engine Conditions, SAE paper 2000-01-0272
- [8] Beatrice, C., *et al.*, An Assessment of Predictivity of CFD Computations of Combustion and Pollutants Formation in DI Diesel Engines, SAE paper 962055
- [9] Yoshizaki, T., Nishida, K., Hiroyasu, H., Three-Dimensional Spray Distributions in a Direct Injection Diesel Engine, SAE paper 941693
- [10] Urlaub, A. G., Chmela FG High-Speed Multi-Fuel Engine: L9204 FMV, SAE paper 740122, 1974
- [11] Mohammadi, A., Kidoguchi, Y., Miwa, K., Effect of Injection Parameters and Wall-Impingement on Atomization and Gas Entrainment Processes in Diesel Sprays, SAE paper 2002-01-0497
- [12] Allocca, L., De Vita, A., Di Angelo, L., Wall-Impingement Analysis of a Spray from a Common Rail Injection System for Diesel Engines, *Proceedings*, THIESEL 2002 Conference on Thermo- and Fluid Dynamic Processes in Diesel Engines, Instituto Motori CNR, Italy, pp. 67-76
- [13] Baumgarten, C., Mixture Formation in Internal Combustion Engines, Springer Verlag, Berlin, 2006
- [14] \*\*\*, AVL FIRE User Manual V. 3; 2006
- [15] Pirouzpanah, V., Kashani, B. O., Prediction of Major Pollutants Emission in Direct-Injection Dual-Fuel Diesel and Natural Gas Engines, SAE paper 1999-01-0841, 1999
- [16] Dukowicz, J. K., Quasi-Steady Droplet Change in the Presence of Convection, Informal Report Los Alamos Scientific Laboratory, LA7997-MS, Los Alamos, N. Mex., USA
- [17] Naber, J. D., Reitz, R. D., Modeling Engine Spray/Wall Impingement, SAE paper 880107
- [18] Mundo, C., Sommerfeld, M., Tropea, C., Droplet-Wall Collisions: Experimental Studies of the Deformation and Breakup Process, *Int. J. Multiphase Flow*, 21 (1995), 2, pp. 151-173
- [19] Mundo, C., Sommerfeld, M., Tropea, C., Experimental Studies of the Deposition and Splashing of Small Liquid Droplets Impinging on a Flat Surface, Paper I-18, ICLASS-94, Rouen, France, 1994

Authors' affiliations:

**S. Jafarmadar (corresponding author)**  
Department of Mechanical Engineering,  
Urmia University 11<sup>th</sup> "Sero" road, Urmia, Iran  
E-mail: s.jafarmadar@urmia.ac.ir

**S. Khalilarya**  
Department of Mechanical Engineering,  
Urmia University Urmia, Iran

**S. Shafee**  
Department of Mechanical Engineering,  
Sahand University of Technology, Tabriz, Iran

**R. Barzegar**  
Department of Mechanical Engineering,  
Urmia University, Urmia, Iran

Paper submitted: November 30, 2008  
Paper revised: April 6, 2009  
Paper accepted: July 19, 2009